



| | |
|-------------------------------|---|
| Publication Year | 2018 |
| Acceptance in OA @INAF | 2022-07-14T14:51:57Z |
| Title | VizieR Online Data Catalog: Highly Accreting Quasars: SDSS Low z Catalog (Negrete+, 2018) |
| Authors | Negrete, C. A.; Dultzin, D.; MARZIANI, Paola; Esparza, D.; Sulentic, J. W.; et al. |
| DOI | 10.26093/cds/vizieR.36200118 |
| Handle | http://hdl.handle.net/20.500.12386/32496 |
| Journal | VizieR Online Data Catalog |


J/A+A/620/A118 Highly Accreting Quasars: SDSS Low z Catalog (Negrete+, 2018)

Highly accreting quasars: The SDSS low-redshift catalog.

Negrete C.A., Dultzin D., Marziani P., Esparza D., Sulentic J. W., del Olmo A., Martínez-Aldama M. L., García-López A., D'Onofrio M, Bon N. Bon E.
<Astron. Astrophys. 620, A118 (2018)>
=2018A&A...620A.118N (SIMBAD/NED BibCode)

ADC_Keywords: Surveys ; QSOs ; Redshifts ; Spectroscopy

Keywords: catalogs - galaxies: active - galaxies: distances and redshifts - galaxies: nuclei - quasars: emission lines - quasars: general

Abstract:

The most highly accreting quasars are of special interest in studies of the physics of active galactic nuclei (AGNs) and host galaxy evolution. Quasars accreting at high rates ($L/L_{\text{Edd}}-1$) hold promise for use as "standard candles": distance indicators detectable at very high redshift. However, their observational properties are still largely unknown.

We seek to identify a significant number of extreme accretors. A large sample can clarify the main properties of quasars radiating near $L/L_{\text{Edd}}-1$ (in this paper they are designated as extreme Population A quasars or simply as extreme accretors) in the $H\beta$ spectral range for redshift ≤ 0.8 .

We use selection criteria derived from four-dimensional Eigenvector 1 (4DE1) studies to identify and analyze spectra for a sample of 334 candidate sources identified from the SDSS DR7 database. The source spectra were chosen to show a ratio R_{FeII} between the FeII emission blend at $\lambda 4570$ and $H\beta$, $R_{\text{FeII}} > 1$. Composite spectra were analyzed for systematic trends as a function of FeII strength, line width, and [OIII] strength. We introduced tighter constraints on the signal-to-noise ratio (S/N) and R_{FeII} values that allowed us to isolate sources most likely to be extreme accretors.

We provide a database of detailed measurements. Analysis of the data allows us to confirm that $H\beta$ shows a Lorentzian function with a full width at half maximum (FWHM) of $H\beta \leq 4000 \text{ km/s}$. We find no evidence for a discontinuity at 2000 km/s in the 4DE1, which could mean that the sources below this FWHM value do not belong to a different AGN class. Systematic [OIII] blue shifts, as well as a blueshifted component in $H\beta$ are revealed. We interpret the blueshifts as related to the signature of outflowing gas from the quasar central engine. The FWHM of $H\beta$ is still affected by the blueshifted emission; however, the effect is non-negligible if the FWHM $H\beta$ is used as a "virial broadening estimator" (VBE). We emphasize a strong effect of the viewing angle on $H\beta$ broadening, deriving a correction for those sources that shows major disagreement between virial and concordance cosmology luminosity values.

The relatively large scatter between concordance cosmology and virial luminosity estimates can be reduced (by an order of magnitude) if a correction for orientation effects is included in the FWHM $H\beta$ value; outflow and sample definition yield relatively minor effects.

Description:

Table 4: contains 103 spectra with an erroneous z identification. The redshift values are given by: the SDSS database (erroneous values), Shen et al. (2011, Cat. [J/ApJS/194/45](#)) and Hewett & Wilde (2010, Cat. [J/MNRAS/405/2302](#)) (correct values).

Table 5: Contains the data described in the Table 2, which are the measurements of the individual spectral fits and derived computations. A detailed description of this table is in Sec. 4.2.

File Summary:

| FileName | Lrecl | Records | Explanations |
|----------------------------|-------|---------|--|
| ReadMe | 80 | . | This file |
| table1.dat | 51 | 101 | Objects with an erroneous z identification |
| table2.dat | 543 | 302 | Measurements of the individual spectral fits |

See also:

[J/MNRAS/405/2302](#) : Improved redshifts for SDSS quasar spectra (Hewett+, 2010)
[J/ApJS/194/45](#) : QSO properties from SDSS-DR7 (Shen+, 2011)

Byte-by-byte Description of file: [table1.dat](#)

| Bytes | Format | Units | Label | Explanations |
|--------|--------|-------|---------|--|
| 1- 19 | A19 | --- | SDSS | SDSS Name |
| 21- 27 | F7.5 | --- | zSDSS | SDSS DR7 redshift |
| 29- 35 | F7.5 | --- | e_zSDSS | SDSS redshift error |
| 37- 43 | F7.5 | --- | zShen | Shen et al. (2011, Cat. J/ApJS/194/45) redshift |
| 45- 51 | F7.5 | --- | zHW | Hewitt & Wilde (2010, Cat. J/MNRAS/405/2302) redshift |

Byte-by-byte Description of file: [table2.dat](#)

| Bytes | Format | Units | Label | Explanations |
|---------|--------|------------------------------|---------------|--|
| 1- 19 | A19 | --- | SDSS | SDSS DR7 designation |
| 21- 27 | F7.5 | --- | z | Redshift considered in this work (1). |
| 29- 35 | F7.5 | --- | e_z | Redshift error |
| 37- 43 | F7.5 | --- | zSDSS | Redshift SDSS DR7 |
| 45- 51 | F7.5 | --- | e_zSDSS | Redshift SDSS DR7 error |
| 53- 57 | F5.2 | --- | S/N | S/N ratio measured around 5100Å |
| 59- 62 | F4.2 | 10-19W/m2/nm | C5100 | Continuum flux at 5100Å in $10^{-17}\text{erg/cm}^2/\text{s}/\text{Å}$ |
| 64- 67 | F4.2 | 10-19W/m2/nm | e_C5100 | Continuum flux at 5100Å error |
| 69- 73 | F5.1 | --- | N5100 | Continuum normalization at 5100Å |
| 75- 79 | F5.2 | --- | e_N5100 | Continuum normalization at 5100Å error |
| 81- 85 | F5.2 | --- | alpha | Power law index |
| 87- 90 | F4.2 | --- | e_alpha | Power law index error |
| 92 | I1 | --- | FaintHG | Faint contribution of the HG |
| 94-101 | F8.2 | 10-20W/m2 | FHbBC | H β _{BC} line flux in $10^{-17}\text{erg/cm}^2/\text{s}$ |
| 103-109 | F7.2 | 10-20W/m2 | e_FHbBC | H β _{BC} line flux error |
| 111-115 | F5.2 | 0.1nm | EWBbBC | H β _{BC} rest-frame equivalent width |
| 117-121 | F5.2 | 0.1nm | e_EWBbBC | H β _{BC} rest-frame equivalent width error |
| 123-127 | I5 | km/s | ShiftHbBC | H β _{BC} shift with respect to the rest-frame |
| 129-133 | F5.1 | km/s | e_ShiftHbBC | H β _{BC} shift with respect to the rest-frame error |
| 135-142 | F8.3 | km/s | FWHMHbBC | H β _{BC} FWHM |
| 144-151 | F8.3 | km/s | e_FWHMHbBC | H β _{BC} FWHM error |
| 153 | A1 | --- | Hbprofile | [GL] G = Gaussian, L = Lorentzian |
| 155-161 | F7.2 | 10-20W/m2 | FHbblue | H β BLUE Line Flux |
| 163-168 | F6.2 | 10-20W/m2 | e_FHbblue | H β BLUE Line Flux error |
| 170-174 | F5.2 | 0.1nm | EWBbblue | H β BLUE rest-frame equivalent width |
| 176-179 | F4.2 | 0.1nm | e_EWBbblue | H β BLUE rest-frame equivalent width error |
| 181-188 | F8.2 | km/s | ShiftHbblue | H β BLUE shift |
| 190-196 | F7.2 | km/s | e_ShiftHbblue | H β BLUE shift error |
| 198-201 | I4 | km/s | FWHMHbblue | H β BLUE FWHM |
| 203-206 | I4 | km/s | e_FWHMHbblue | H β BLUE FWHM error |
| 208-215 | F8.2 | 10-20W/m2 | FFeII | FeII flux |
| 217-223 | F7.2 | 10-20W/m2 | e_FFeII | FeII flux error |
| 225-230 | F6.2 | 0.1nm | EWFeII | FeII rest-frame equivalent width |
| 232-235 | F4.1 | 0.1nm | e_EWFeII | FeII rest-frame equivalent width error |
| 237-240 | A4 | --- | Pop | Population designation |
| 242-246 | F5.3 | --- | RFeII | Ratio between the FeII emission blend at $\lambda 4570$ and H β |
| 248-252 | F5.3 | --- | e_RFeII | RFeII error |
| 254-259 | F6.3 | --- | AIHb | H β asymetry (only objects with Hbblue) |
| 261-265 | F5.3 | --- | e_AIHb | H β asymetry error |
| 267-270 | F4.2 | --- | Kurt | Kurtosis |
| 272-275 | F4.2 | --- | e_Kurt | Kurtosis error |
| 277-281 | I5 | km/s | C010 | H β centroid at 0.10 of the line intensity |
| 283-286 | I4 | km/s | e_C010 | H β centroid at 0.10 of the line intensity error |
| 288-291 | I4 | km/s | C025 | H β centroid at 0.25 of the line intensity |
| 293-295 | I3 | km/s | e_C025 | H β centroid at 0.25 of the line intensity error |
| 297-300 | I4 | km/s | C050 | H β centroid at 0.50 of the line intensity |
| 302-304 | I3 | km/s | e_C050 | H β centroid at 0.50 of the line intensity error |
| 306-309 | I4 | km/s | C075 | H β centroid at 0.75 of the line intensity |
| 311-313 | I3 | km/s | e_C075 | H β centroid at 0.75 of the line intensity error |
| 315-318 | I4 | km/s | C090 | H β centroid at 0.90 of the line intensity |
| 320-322 | I3 | km/s | e_C090 | H β centroid at 0.90 of the |

| | | | | |
|---------|------|---------------------------|---------------|--|
| | | | | line intensity error |
| 324-329 | F6.2 | 10-20W/m2 | FHeII | HeII line flux |
| 331-335 | F5.2 | 10-20W/m2 | e_FHeII | HeII line flux error |
| 337-344 | F8.2 | km/s | ShiftHeII | HeII shift with respect to the rest frame |
| 346-352 | F7.2 | km/s | e_ShiftHeII | HeII shift with respect to the rest frame error |
| 354-357 | I4 | km/s | FWHMHeII | HeII FWHM |
| 359-362 | I4 | km/s | e_FWHMHeII | HeII FWHM error |
| 364-369 | F6.2 | 10-20W/m2 | FHbNC | H β _{NC} Line Flux |
| 371-375 | F5.2 | 10-20W/m2 | e_FHbNC | H β _{NC} Line Flux error |
| 377-380 | F4.2 | 0.1nm | EWbNC | H β _{NC} rest-frame equivalent width |
| 382-385 | F4.2 | 0.1nm | e_EWbNC | H β _{NC} rest-frame equivalent width error |
| 387-388 | I2 | km/s | ShiftHbNC | H β _{NC} shift with respect to the rest-frame |
| 390-394 | F5.1 | km/s | e_ShiftHbNC | H β _{NC} shift with respect to the rest-frame error |
| 396-399 | I4 | km/s | FWHMHbNC | H β _{NC} FWHM |
| 401-403 | I3 | km/s | e_FWHMHbNC | H β _{NC} FWHM error |
| 405-411 | F7.2 | 10-20W/m2 | FOIII | Line flux of [OIII] 5007 |
| 413-419 | F7.2 | 10-20W/m2 | e_FOIII | Line flux error of [OIII] 5007 |
| 421-425 | F5.2 | 0.1nm | EWIII | Line [OIII] 5007 rest-frame equivalent width |
| 427-431 | F5.2 | 0.1nm | e_EWIII | Line [OIII] 5007 rest-frame equivalent width error |
| 433-440 | F8.2 | km/s | ShiftOIII | Line [OIII] 5007 shift with respect to the rest-frame |
| 442-447 | F6.2 | km/s | e_ShiftOIII | Line [OIII] 5007 shift with respect to the rest-frame error |
| 449-452 | I4 | km/s | FWHMOIII | Line [OIII] 5007 FWHM |
| 454-457 | I4 | km/s | e_FWHMOIII | Line [OIII] 5007 FWHM error |
| 459-465 | F7.2 | 10-20W/m2 | FOIIISB | Semi broad line [OIII] 5007 flux |
| 467-473 | F7.2 | 10-20W/m2 | e_FOIIISB | Semi broad line [OIII] 5007 flux error |
| 475-479 | F5.2 | 0.1nm | EWIIISB | Semi broad line [OIII] 5007 rest-frame equivalent width |
| 481-485 | F5.2 | 0.1nm | e_EWIIISB | Semi broad line [OIII] 5007 rest-frame equivalent width error |
| 487-494 | F8.2 | km/s | ShiftOIIISB | Semi broad line [OIII] 5007 shift with respect to the rest frame |
| 496-501 | F6.2 | km/s | e_ShiftOIIISB | Semi broad line [OIII] 5007 shift with respect to the rest frame error |
| 503-506 | I4 | km/s | FWHMOIIISB | Semi broad line [OIII] 5007 FWHM |
| 508-511 | I4 | km/s | e_FWHMOIIISB | Semi broad line [OIII] 5007 FWHM error |
| 513-516 | F4.2 | [Msun] | logMBH | Black hole mass |
| 518-521 | F4.2 | [Msun] | e_logMBH | Black hole mass error |
| 523-527 | F5.2 | [Lsun] | logLbol | Bolometric luminosity |
| 529-532 | F4.2 | [Lsun] | e_logLbol | Bolometric luminosity error |
| 534-538 | F5.2 | --- | L/LEdd | Eddington ratio |
| 540-543 | F4.2 | --- | e_L/LEdd | Eddington ratio error |

Note (1): measured using the H β _{NC} or [OIII] λ 5007 line (see text).

Acknowledgements:






Alenka Negrete, alenka(at)astro.unam.mx

(End)

Patricia Vannier [CDS] 10-Sep-2018

The document above follows the rules of the [Standard Description for Astronomical Catalogues](#); from this documentation it is possible to generate *f77* program to load files [into arrays](#) or [line by line](#)

© Université de Strasbourg/CNRS

     Contact 